Pinning of hidden vortices in Bose-Einstein condensates

T. Mithun,[1] K. Porsezian,[1] and Bishwajyoti Dey[2]
[1]*Department of Physics, Pondicherry University, Puducherry 605014, India*
[2]*Department of Physics, University of Pune, Pune 411007, India*
(Received 19 February 2014; published 28 May 2014)

We study the vortex dynamics and vortex pinning effect in Bose-Einstein condensates in a rotating double-well trap potential and corotating optical lattice. We show that the vortex number does not diverge when the rotational frequency $\Omega \to 1$ if the trap potential is of anisotropic double-well type. The critical rotational frequency as obtained from numerical simulations agrees very well with the value $\sqrt{l}/l$ for $l = 4$, which supports the conjecture that surface modes with angular momentum $l = 4$ are excited when the rotating condensate is trapped in a double-well potential. The vortex lattice structure in a rotating triple-well trap potential and its pinning show very interesting features. We show the existence and pinning of hidden vortices whose phase profile is similar to that of the visible vortices.

DOI: 10.1103/PhysRevA.89.053625 PACS number(s): 03.75.Lm, 03.75.Kk, 67.85.Hj

One of the most striking properties of the rotating Bose-Einstein condensate (BEC) is its ability to form vortices and a vortex lattice that manifest the superfluidity of the BEC [1]. Ultracold gases in optical lattices can be used to explore a wide range of fundamental problems in condensed matter physics [2]. Inspired by this, extensive theoretical and experimental studies have taken place with BECs in rotating optical lattices showing some interesting properties [3]. Pinning of vortices and the associated structural phase transition from the Abrikosov vortex lattice structure to the lattice structure of the optical lattice is one of those properties [4–9].

The BEC in a double-well potential trap has received much attention because of its rich physics [10–14]. This has motivated the study of the BEC trapped in a rotating double-well potential [15]. A recent theoretical study about the Feynman rule for the number of vortices in a rotating superfluid applied to a BEC trapped in a rotating double-well potential has unearthed the existence of hidden vortices [16]. These hidden vortices do not have visible cores but carry angular momentum. It has been shown that the Feynman rule for the number of vortices in the condensate can be satisfied only after including the hidden vortices [16,17].

Our study is motivated by the report of hidden vortices in a BEC in a rotating double-well trap potential [16]. It is natural to ask whether the hidden vortices can be pinned by the optical lattice. In this paper we study the vortex formation and vortex pinning in a BEC in a rotating double-well trap potential and corotating optical lattice. Interestingly, our numerical simulations show that there exist two types of hidden vortices with different phase profiles and only the type that displays a phase profile similar to that of the visible vortices can be pinned to the optical lattice. Since the hidden vortices are distributed along the central barrier region of the double-well trap potential, we consider the case of a triple-well trap potential where there are two barrier regions. In this case the nature of the vortex lattice and its pinning effect shows very interesting features. Another motivation for the present study is to derive the Feynman rule for a BEC trapped in an anisotropic double-well potential. The Feynman rule for the number of vortices N in a rotating superfluid in a rigid container of radius R is given by $N = m\Omega R^2/\hbar$ [18]. It has been shown that for a condensate trapped in a single-well (harmonic) potential and confined in a corotating optical lattice, the number of vortices increases linearly with rotational frequency Ω and diverges when the rotational frequency approaches the harmonic trap frequency [19]. However, no such divergence in the vortex number has been observed in the experiments of Williams *et al* [6]. Subsequently Kato *et al.* [7] argued that such divergence in the number of vortices could be avoided if one considers an optical lattice with a Gaussian envelope of the laser beams. We show that the nondivergence of the number of vortices for $\Omega \to 1$ also occurs if the BEC is trapped in an anisotropic double-well potential. We have also addressed the problem of the relation between the surface-mode frequency and the critical rotational frequency Ω_c for rotating a BEC in a double-well trap potential. For the case of a harmonic trap (single-well) potential the initial surface-mode excitation that leads to single-vortex formation has angular momentum $l = 2$. However, for the case of a double-well trap potential, the problem is nontrivial as in this case it is conjectured that higher-order surface modes with $l = 4$ are expected to contribute to the initial motion of the rotating condensate that leads to the vortex formation [17].

We consider the two-dimensional (2D) dimensionless time-dependent Gross-Pitaevskii equation (GPE) $(i - \gamma)\psi_t = [-\frac{1}{2}(\nabla_x^2 + \nabla_y^2) + V(x,y) - \mu + p|\psi|^2 - \Omega L_z]\psi$ [5] for the formulation of our problem. The potential $V(x,y)$ is the sum of two potentials $V_{\rm DW}(x,y) + V_{\rm lattice}(\mathbf{r})$. Here $V_{\rm DW}(x,y)$ is the anisotropic double-well trap potential given by $V_{\rm DW}(x,y) = \frac{1}{2}(x^2 + \lambda^2 y^2) + V_0 e^{-x^2/2\sigma^2}$, where V_0 denotes the depth of the double-well potential and $\lambda = \omega_y/\omega_x$ denotes the anisotropy parameter; $V_{\rm lattice}$ denotes the optical lattice potential and is given by

$$V_{\rm lattice}(\mathbf{r}) = \sum_{n_1,n_2} V_1 \exp\left(-\frac{|\mathbf{r} - \mathbf{r}_{n_1,n_2}|^2}{(\sigma'/2)^2}\right).$$

Here $\mathbf{r}_{n_1,n_2} = n_1\mathbf{a}_1 + n_2\mathbf{a}_2$ denotes the lattice points and V_1 is the strength of the laser beam. For the triangular optical lattice (TOL), the two lattice unit vectors are given by $\mathbf{a}_1 = a(1,0)$ and $\mathbf{a}_2 = a(-1/2, \sqrt{3}/2)$, whereas for the square optical lattice (SOL) $\mathbf{a}_1 = a(1,0)$ and $\mathbf{a}_2 = a(0,1)$. The spatial coordinates, time, condensate wave function, and rotational frequency are in units of a_0, ω_x^{-1}, and $a_0^{-3/2}$, and ω_x, respectively, where

$a_0 = \sqrt{\hbar/m\omega_x}$. The strength of the potentials V_0 and V_1 are in units of $\hbar\omega_x$. The two-body interaction parameter p is given by $p = 4\pi a_s \mathbb{N}/R_z$, where a_s is the s-wave scattering length, $\mathbb{N}$ is the total number of particles, and R_z is the condensate size along the z direction. In addition, μ is the chemical potential and γ is the phenomenological dissipation parameter. The dissipation term enables the system to relax into an equilibrium configuration. The value of the dissipation parameter γ has been determined by fitting theoretical results with experiments to be 0.03. We have used the same value in our calculations. Small variation of γ only influences the relaxation time scale, but does not change the ultimate steady-state vortex structure. For discussions on the dissipation mechanism see [20,21].

The Crank-Nicolson scheme is used to numerically solve the 2D GPE. For our simulation, we set a small spatial step $\Delta x = \Delta y = 0.04$ and time step $\Delta t = 0.0005$. The dissipation parameter is set to $\gamma = 0.03$. The lattice constant a is fixed as $a = 2.2$ and $p = 1000$. The parameters are chosen from the experiments of ^{87}Rb [6,7]. All the quantities plotted in the figures are dimensionless.

We obtain below the expression for the surface-mode frequency for the rotating condensates trapped in a double-well potential using the time-dependent variational analysis. For this we set $V_{\text{lattice}}(\mathbf{r}) = 0$ and $\lambda = 1$. As the condensate is trapped in the double-well-shaped potential, we use the ansatz for the condensate wave function to be of the form

$$\psi(x,y,t) = c(t)x^2 \exp\{-\tfrac{1}{2}[\alpha(t)x^2 + \beta(t)y^2 - 2i\gamma(t)xy]\}.$$

In the presence of rotation, the centrifugal term $-\Omega L_z$ shifts the surface mode with $l = 4$ (for the double-well trap potential) by $\pm 4\Omega$. By following a similar procedure for finding the surface-mode frequency for the harmonic trap potential case [22], we obtain the lowest-energy surface-mode frequency for a BEC trapped in a rotating double-well potential as $\omega_{-4} = \omega - 4\Omega$ [23]. This relation shows that the dynamical instability that leads to the visible vortex formation begins at $\Omega = \omega/4$. Table I shows the variation of the surface-mode frequency $\Omega = \omega/4$ and the critical rotational frequency Ω_c obtained numerically with nonlinear interaction parameter p and the depth of the double-well potential V_0. It can be seen that Ω_c agrees quite well with the value $\sqrt{l}/l = 0.5$ for $l = 4$. This shows that the initial condensate motion that leads to the vortex formation indeed consists of the higher-order surface modes with $l = 4$. The comparison between the two frequencies shows that the surface-mode frequency is much smaller than Ω_c. This is unlike the harmonic (single-well) trap case, where the surface-mode frequency is quite close to Ω_c [22].

TABLE I. Surface mode frequency Ω and critical rotational frequency Ω_c.

	Theoretical $\Omega = \omega/4$		Numerical Ω_c	
p	$V_0 = 40$	$V_0 = 20$	$V_0 = 40$	$V_0 = 20$
1000	0.258	0.220	0.47	0.46
800	0.279	0.237	0.49	0.48
600	0.307	0.260	0.52	0.52
400	0.346	0.297	0.57	0.56
200	0.402	0.359	0.62	0.63

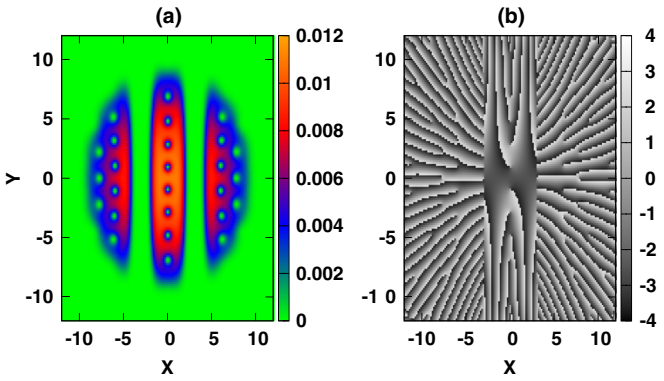

FIG. 1. (Color online) (a) Condensate density $|\psi^2|$ for a triple-well trap and (b) phase profile of ψ for $\Omega = 0.9$ at $t = 300$. Here $V_0 = 40$ and $\sigma = 0.5$.

Figure 1(a) shows the vortex lattice formation in a BEC trapped in a symmetric triple-well potential given by $V_{\text{TW}}(x,y) = \frac{1}{2}(x^2 + y^2) + V_0 e^{-(x+3)^2/2\sigma^2} + V_0 e^{-(x-3)^2/2\sigma^2}$. In the central potential well, the vortices form a one-dimensional linear chain structure. However, in the two other wells on both sides of the central well, the vortex lattice structure is the usual Abrikosov lattice. The hidden vortices that form in the two barrier regions around the central potential well are shown as phase defects in the corresponding phase profile in Fig. 1(b). We have also confirmed numerically the presence of the hidden vortices in this case from the Feynman rule, which can also be written as $N_t/2 = l_z$, where N_t is the total number of vortices (visible plus hidden) in the condensate and l_z is the average angular momentum per atom in equilibrium [18,19,21].

We derive the Feynman rule for the rotating BEC when trapped in an anisotropic double-well potential $V_{\text{DW}} = \frac{1}{2}m(\omega_x^2 x^2 + \omega_y^2 y^2) + V_0 e^{-x^2/2\alpha^2}$. The effective potential in the presence of the rotation is

$$V(\Omega) = \frac{m}{2}\omega_x^2 x^2\left(1 - \frac{\Omega^2}{\omega_x^2} - \frac{V_0}{m\omega_x^2\alpha^2}\right) + \frac{1}{2}\omega_y^2 y^2\left(1 - \frac{\Omega^2}{\omega_y^2}\right) + V_0,$$

where we have retained terms only up to second order in x/α. Using the Thomas-Fermi approximation, we neglect the kinetic energy term in the Gross-Pitaevskii equation [19] to get

$$\mu'_{\text{TF}}(\Omega) = \frac{m}{2}\omega_x^2 R_x^2(\Omega)\left(1 - \frac{\Omega^2}{\omega_x^2} - a\right) + \frac{1}{2}m\omega_y^2 R_y^2(\Omega)\left(1 - \frac{\Omega^2}{\omega_y^2}\right).$$

Here $\mu'_{\text{TF}}(\Omega) = \mu_{\text{TF}}(\Omega) - V_0$, $\mu'_{\text{TF}}(0) = \mu_{\text{TF}}(0) - V_0$, and $a = \frac{V_0}{m\omega_x^2\alpha^2}$. The radius of the condensate can be taken as the average of the condensate radius along the x and y directions as $R(\Omega)^2 = \frac{1}{2}[R_x^2(\Omega) + R_y^2(\Omega)]$, where $R_x(\Omega)$ $[R_y(\Omega)]$ can be obtained by putting $R_y(\Omega) = 0$ $[R_x(\Omega) = 0]$ in the above

expression of $\mu'_{\rm TF}(\Omega)$. We thus obtain

$$R(\Omega)^2 = \frac{\mu'_{\rm TF}(\Omega)}{m}\left(\frac{1}{\left(1-\frac{\Omega^2}{\omega_x^2}-a\right)\omega_x^2}+\frac{1}{\left(1-\frac{\Omega^2}{\omega_y^2}\right)\omega_y^2}\right).$$

The normalization condition $\int \psi^*\psi\, dx\, dy = 1$ gives the relation between $\mu'_{\rm TF}(\Omega)$ and $\mu'_{\rm TF}(0)$ as $\mu'_{\rm TF}(\Omega)/\mu'_{\rm TF}(0) = (\Lambda)^{1/4}$, where

$$\Lambda = \left(\frac{\left(1-\frac{\Omega^2}{\omega_x^2}-a\right)\left(1-\frac{\Omega^2}{\omega_y^2}\right)}{(1-a)}\right).$$

Using this relation and the values of $R_x(0)$ and $R_y(0)$ as obtained above, the condensate radius can be written as

$$R(\Omega)^2 = \frac{\Lambda}{2}\left(\frac{(1-a)R_x(0)^2}{1-a-\frac{\Omega^2}{\omega_x^2}}+\frac{\lambda^2 R_y(0)^2}{\lambda^2-\frac{\Omega^2}{\omega_x^2}}\right),$$

where $\lambda = \frac{\omega_y}{\omega_x}$. We thus obtain the Feynman rule for the double-well trap potential in our dimensionless unit as $N = \Omega R^2(\Omega)$, where

$$R^2(\Omega) = \frac{\Lambda}{2}\left[R_x^2(0)\left(\frac{1-b}{1-b-\Omega^2}\right)+R_y^2(0)\left(\frac{\lambda^2}{\lambda^2-\Omega^2}\right)\right],$$

$b = V_0/\sigma^2$, $\sigma = \alpha/a_0$, and

$$\Lambda = \left(\frac{(1-\Omega^2-b)(1-\Omega^2/\lambda^2)}{1-b}\right)^{1/4}.$$

Here $R_x(0)$ and $R_y(0)$ are the condensate radii along the x and y directions, respectively, in the ground state. For a harmonic symmetric trap $b = 0$, $\lambda = 1$, $R_x = R_y = R_\perp$, $\Lambda = (1-\Omega^2)^{1/2}$, and we get back the result $R^2(\Omega) = R_\perp(0)^2 (1-\Omega^2)^{-1/2}$ [7].

From the Feynman rule as derived above, it could be seen that for the isotropic case ($\lambda = 1$) the radius of the condensate $R(\Omega) \to \infty$ when $\Omega \to 1$, similar to the case of the harmonic trap. On the other hand, for the anisotropic case ($\lambda \neq 1$) the radius of the condensate depends on the anisotropy parameter λ. Whenever $\lambda < 1$, the term $\lambda^2 - \Omega^2$ becomes negative and the condensate becomes unstable. However, for $\lambda > 1$ the rotation at $\Omega = 1$ is also possible. This is shown in Fig. 2. It could be seen from the figure that the analytical Feynman rule for the number of vortices matches quite well the total number of vortices N_t as obtained numerically. It may be noted that for $\lambda > 1$, the divergence is shifted to $\Omega > 1$. Because of this it is now possible to rotate the cloud at a frequency above the critical value $\Omega = 1$. However, experimentally there is a limit to which the rotational frequency can be increased beyond the value $\Omega = 1$ because of the increased heating of the condensate, which leads to a drop in the number of vortices. For example, in Ref. [6] the vortices could be observed only up to $\frac{\Omega}{\omega_r} = 1.15$. Therefore, the anisotropy parameter $\lambda = \frac{\omega_y}{\omega_x}$ can be appropriately adjusted to shift the divergence to a frequency value that is beyond the experimental limit of the rotational frequency Ω.

In Fig. 3 we present the lattice potential energy obtained from numerical simulations for different strengths V_1 of the TOL (red points) and SOL (blue line with points). It shows that the transition from the Abrikosov vortex lattice to the pinned

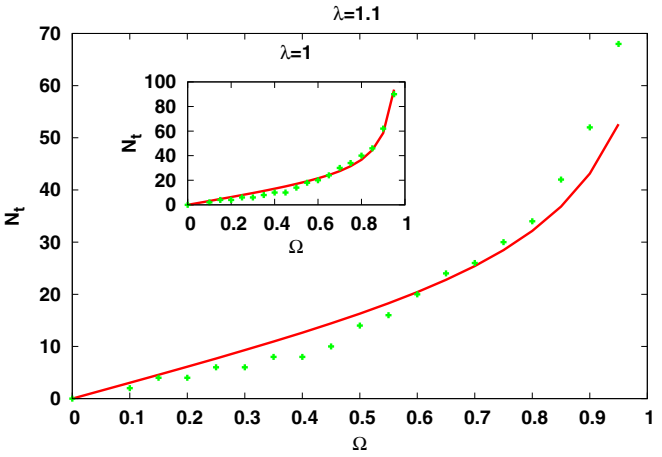

FIG. 2. (Color online) Variation of the total number of vortices with rotational frequency Ω. The solid line represents analytical results and the points represent the numerical results for $\lambda = 1.1$. The inset shows the isotropic case $\lambda = 1$. Here $V_0 = 40$ and $\sigma = 0.5$.

lattice occurs through the intermediate coexisting state, similar to that observed for the case of the harmonic trap potential [5]. The comparison between the two cases shows that the strength of the TOL potential required for the pinning of the visible vortices is lower than that of the SOL case. This is expected since the Abrikosov vortex lattice structure is commensurate with the TOL. Figure 4(a) shows the completely pinned vortex lattice for the SOL with strength $V_1 = 2.2$. When the strength of the SOL is further increased to $V_1 = 3$, we find that there is an extra unpinned vortex on both sides of the central barrier region as shown in Fig. 4(b). A defect of this kind has already been observed in an experiment for the BECs trapped in a harmonic potential [4]. It is interesting to note that such defects do not appear for the TOL (not shown here). This is because of the commensurate nature of the Abrikosov vortex lattice and the TOL, which allows all the vortices to get pinned to the optical lattice pinning sites, leaving no room for unpinned defect vortices.

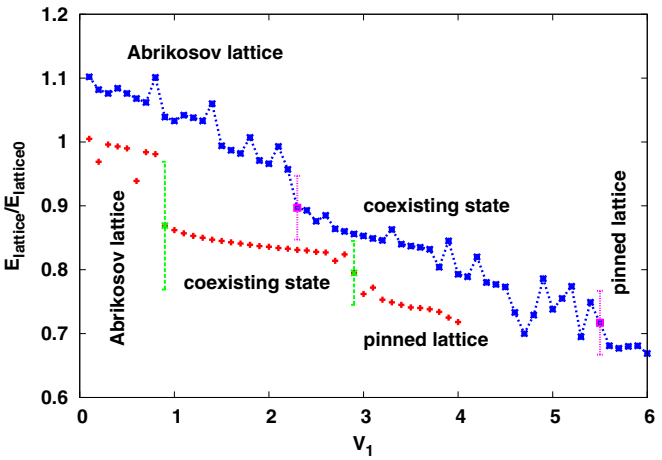

FIG. 3. (Color online) Lattice potential energy against the strength V_1 of the TOL (red points) and SOL (blue line with points). Here $\Omega = 0.7$, $V_0 = 40$, and $\sigma = 0.5$.

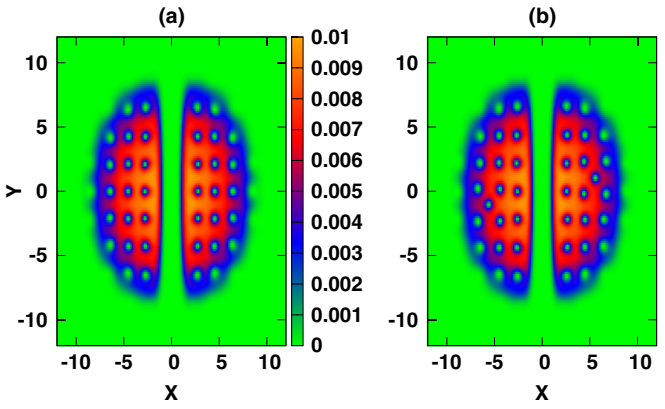

FIG. 4. (Color online) Pinned vortex lattice for the SOL potential at (a) $V_1 = 2.2$ and (b) $V_1 = 3$ and $t = 250$. Here $\Omega = 0.9$ and $\sigma = 0.5$.

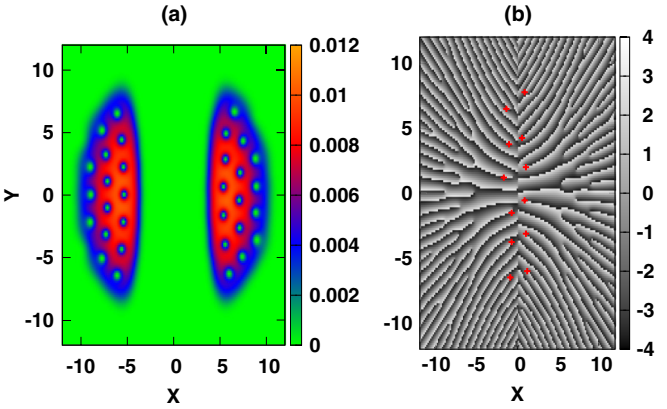

FIG. 6. (Color online) (a) Condensate density and (b) its phase profile. Here $\Omega = 0.9$, $V_1 = 0$, and $\sigma = 2$.

Figure 5 shows the pinning of the vortices for the case of rotating a BEC in a triple-well trap potential. Due to the linear lattice structure of the vortex lattice [see Fig. 1(a)], only alternate vortex sites in the linear chain of vortices coincide with the pinning sites of the TOL and can get pinned. This is exactly shown by our numerical simulation and in Fig. 5(a), where we can see that only alternate vortices of the central linear chain of vortices are pinned. The vortices in the neighboring two wells form the usual Abrikosov lattice and therefore all these are pinned to the TOL. On the other hand, all the vortex sites in the linear chain of vortices coincide with the SOL pinning sites and can get pinned. This is shown in Fig. 5(b), where we can see that all the vortices in the central well are completely pinned. In the neighboring two wells, all the vortices are also pinned, except the defect vortices.

We now consider the pinning of the hidden vortices. This is a difficult problem because the pinning, if any, could be seen only as defects in the phase profile of the condensate density. To get a clear picture of the pinning of hidden vortices, we first increase the number of hidden vortices in the condensate. This can be done by adequately increasing the width of the central barrier region of the double-well trap potential (by increasing σ) such that this region can accommodate a sufficient number of hidden vortices. Interestingly, by increasing the width, we find the existence of a different type of hidden vortex located in the central barrier region. The phase profile of this type of hidden vortex is different from that of the hidden vortices reported earlier in the literature [16]. Figure 6(a) shows the visible vortices that form the usual Abrikosov lattice on both sides of the larger central barrier region. From the phase profile in Fig. 6(b) we can see that there are two types of such phase defects in the central barrier region. There are some lines that end in the central barrier line where the phase changes discontinuously and these defects are the usual hidden vortices reported earlier in the literature. Then there are other lines where the phase changes discontinuously from black to white (similar to the phase profile of the visible vortices) and the end of these lines represent the phase defects. These phase defects [shown by red points in Fig. 6(b)] represent a different type of hidden vortex. We identify these phase defects as hidden vortices since there are no visible vortices at these positions (red points) as seen from Fig. 6(a). This is also checked by calculating the average value of the angular momentum and verifying the Feynman $N_t/2 = l_z$ rule as mentioned above. From numerical simulations we find that only this type of hidden vortex gets pinned to the optical lattice sites. Figure 7(a) shows the pinning of the visible vortices in the SOL potential. Figure 7(b) shows the

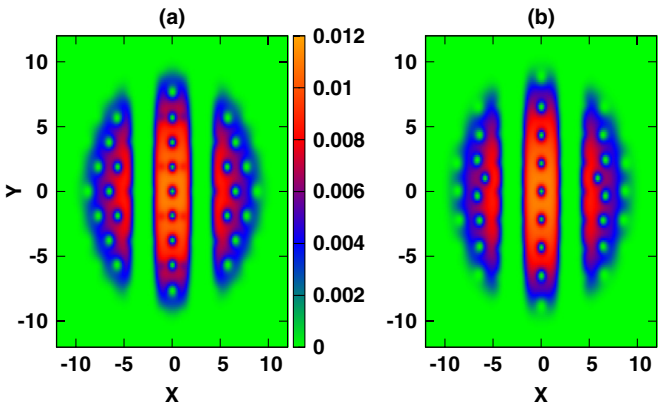

FIG. 5. (Color online) Pinned vortex lattice for the (a) TOL and (b) SOL potentials. Here $p = 1000$, $\Omega = 0.9$, $V_1 = 3$, and $\sigma = 0.5$.

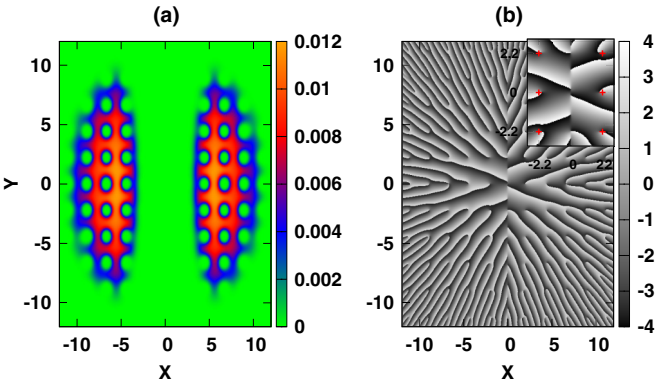

FIG. 7. (Color online) (a) Pinned vortex lattice for the SOL potential and (b) its phase profile. Here $\Omega = 0.9$, $V_1 = 100$, and $\sigma = 2$.

corresponding phase profile. As we increase the strength of the SOL potential, the hidden vortices gradually move away from their positions and finally get pinned to the SOL sites. The magnified picture of the central region is shown in the right top corner of the figure, where the pinned hidden vortices are shown by red points. Similar pinning of the hidden vortices is also seen for the TOL for lattice strength $V_1 = 100$.

In conclusion, we have derived analytically the surface-mode frequency and the Feynman rule for the BEC in a rotating double-well trap potential and compared them with numerical results. We have shown the existence of the surface mode with $l = 4$ for the double-well potential and the nondivergence of the vortex number for the anisotropic double-well potential when $\Omega \to 1$. The linear vortex lattice structure as well as its interesting pinning effect for the condensate in a rotating triple-well trap potential is expected to be very useful in applications such as quantum computing [24]. We have shown the existence of hidden vortices whose phase profile is similar to that of the visible vortices. It is shown that this type of hidden vortex also gets pinned, but for a much higher strength of the optical lattice.

B.D. thanks DST and BCUD-PU for financial support through research projects. K.P. thanks DST, CSIR, and UGC for financial support through research projects.

[1] M. R. Matthews, B. P. Anderson, P. C. Haljan, D. S. Hall, C. E. Wieman, and E. A. Cornell, Phys. Rev. Lett. **83**, 2498 (1999); K. W. Madison, F. Chevy, W. Wohlleben, and J. Dalibard, *ibid.* **84**, 806 (2000); J. R. Abo-Shaeer, C. Raman, J. M. Vogels, and W. Ketterle, Science **292**, 476 (2001); A. Aftalion and Q. Du, Phys. Rev. A **64**, 063603 (2001).

[2] M. Greiner, O. Mandel, T. Esslinger, T. W. Hänsch, and I. Bloch, Nature (London) **415**, 39 (2002); J. Billy, V. Josse, Z. Zuo, A. Bernard, B. Hambrecht, P. Lugan, D. Clement, L. Sanchez-Palencia, P. Bouyer, and A. Aspect, *ibid.* **453**, 891 (2008); G. Roati, C. D'Errico, L. Fallani, M. Fattori, C. Fort, M. Zaccanti, G. Modugno, M. Modugno, and M. Inguscio, *ibid.* **453**, 895 (2008); T. Kinoshita, T. Wenger, and D. S. Weiss, Science **305**, 1125 (2004).

[3] M. Polini, R. Fazio, A. H. MacDonald, and M. P. Tosi, Phys. Rev. Lett. **95**, 010401 (2005); R. N. Palmer and D. Jaksch, *ibid.* **96**, 180407 (2006); R. Bhat, M. Krämer, J. Cooper, and M. J. Holland, Phys. Rev. A **76**, 043601 (2007).

[4] S. Tung, V. Schweikhard, and E. A. Cornell, Phys. Rev. Lett. **97**, 240402 (2006).

[5] T. Sato, T. Ishiyama, and T. Nikuni, Phys. Rev. A **76**, 053628 (2007).

[6] R. A. Williams, S. Al-Assam, and C. J. Foot, Phys. Rev. Lett. **104**, 050404 (2010).

[7] A. Kato, Y. Nakano, K. Kasamatsu, and T. Matsui, Phys. Rev. A **84**, 053623 (2011).

[8] H. Pu, L. O. Baksmaty, S. Yi, and N. P. Bigelow, Phys. Rev. Lett. **94**, 190401 (2005); R. Bhat, L. D. Carr, and M. J. Holland, *ibid.* **96**, 060405 (2006).

[9] K. Kasamatsu and M. Tsubota, Phys. Rev. Lett. **97**, 240404 (2006).

[10] M. Albiez, R. Gati, J. Fölling, S. Hunsmann, M. Cristiani, and M. K. Oberthaler, Phys. Rev. Lett. **95**, 010402 (2005); S. Levy, E. Lahoud, I. Shomroni, and J. Steinhauer, Nature (London) **449**, 579 (2007).

[11] B. Xiong, J. Gong, H. Pu, W. Bao, and B. Li, Phys. Rev. A **79**, 013626 (2009).

[12] B. Juliá-Díaz, M. Melé-Messeguer, M. Guilleumas, and A. Polls, Phys. Rev. A **80**, 043622 (2009).

[13] R. W. Spekkens and J. E. Sipe, Phys. Rev. A **59**, 3868 (1999).

[14] J. R. Salgueiro, M. Zacarés, H. Michinel, and A. Ferrando, Phys. Rev. A **79**, 033625 (2009).

[15] S. Hofferberth, I. Lesanovsky, B. Fischer, J. Verdu, and J. Schmiedmayer, Nat. Phys. **2**, 710 (2006).

[16] L. H. Wen, H. Xiong, and B. Wu, Phys. Rev. A **82**, 053627 (2010).

[17] L. H. Wen and X. B. Luo, Laser Phys. Lett. **9**, 618 (2012).

[18] R. P. Feynman, Prog. Low Temp. Phys. **1**, 17 (1955).

[19] A. L. Fetter, Rev. Mod. Phys. **81**, 647 (2009).

[20] M. Tsubota, K. Kasamatsu, and M. Ueda, Phys. Rev. A **65**, 023603 (2002).

[21] K. Kasamatsu, M. Tsubota, and M. Ueda, Phys. Rev. A **67**, 033610 (2003).

[22] T. Mithun, K. Porsezian, and B. Dey, Phys. Rev. E **88**, 012904 (2013).

[23] Here ω is derived as $\omega^2 = 4 - \frac{7\alpha_{10}^3+35\beta_{10}^3}{15} - \frac{p(7\alpha_{10}^3+35\beta_{10}^3)}{192\sqrt{\alpha_{10}\beta_{10}}\pi} - \frac{p\sqrt{\alpha_{10}\beta_{10}}(7\alpha_{10}+35\beta_{10})}{192\pi} - \frac{V_0\beta_{10}^4\sqrt{2\alpha_{10}\beta_{10}}(32\alpha_{10}^4\sigma^7-12\alpha_{10}^3\sigma^5)}{(\beta_{10}+2\alpha_{10}\beta_{10}\sigma^2)^{9/2}}$.

[24] K. T. Kapale and J. P. Dowling, Phys. Rev. Lett. **95**, 173601 (2005).